Measurement of Solute Partitioning across Liquid/Liquid Interfaces Using Scanning Electrochemical Microscopy−Double Potential Step Chronoamperometry (SECM−DPSC): Principles, Theory, and Application to Ferrocenium Ion Transfer Across the 1,2-Dichloroethane/Aqueous Interface

Anna L. Barker and Patrick R. Unwin*

Department of Chemistry, University of Warwick, Coventry CV4 7AL, U.K.

Received: February 14, 2001; In Final Form: July 23, 2001

SECM−DPSC is extended as an approach for probing the transfer of a target electrogenerated species across the interface between two immiscible phases, by developing a theoretical model for reversible phase transfer. The SECM−DPSC technique involves the electrogeneration of a target species at an UME positioned close to an interface in an initial (forward) potential step. After a defined period, this species is then collected back at the UME by reversing the potential step. The numerical treatment for calculating the UME current−time response during the forward and reverse potential steps is outlined, without restriction on the partition coefficient of the solute between the two phases, thereby building on an earlier model (Slevin, C. J.; Macpherson, J. V.; Unwin, P. R. *J. Phys. Chem. B* **1997**, *101*, 10851). It is shown that the technique can be used to measure both the partition coefficient and kinetics of phase transfer. The approach is illustrated through experimental studies of the transfer of the oxidized form of ferrocene (Fc) and derivatives across a 1,2-dichloroethane (DCE)/aqueous interface, with ClO_4^- present in excess in each phase. The transfer of ferrocenium and dimethylferrocenium, accompanied by ClO_4^- to maintain charge neutrality, are both found to be diffusion limited (rate constants > 0.5 cm s^{-1}), even on the fastest time scales accessible with SECM. In contrast, decamethylferrocenium ion does not appear to transfer across the interface under the defined conditions. In certain cases, such as slightly elevated temperatures, UME oxidation of ferrocene derivatives in the vicinity of the DCE/aqueous interface, was found to be accompanied by interfacial instabilities akin to a Marangoni phenomenon. SECM may provide a new method for initiating and monitoring such effects.

Introduction

Conventional electrochemical techniques for investigating electron transfer (ET) across the interface between two immiscible electrolyte solutions (ITIES), such as cyclic voltammetry[1−6] and ac impedance,[7,8] essentially involve the measurement of total charge transferring across the liquid/liquid interface and so discrimination between ET and coupled ion transfer (IT) processes is difficult. It is therefore desirable, when using these techniques, to choose systems where the ET and IT processes occur at well separated potentials so that ET can be probed without interference due to IT. Even with scanning electrochemical microscopy (SECM) studies of ET kinetics at ITIES,[9] it is important to ensure that there is no transfer of any components of the redox couples across the interface, so that the ET process is purely heterogeneous.

The extent to which a chemical species partitions between two immiscible phases depends on its structure and charge, as well as the polarity of the solvents and the nature and concentration of the supporting electrolyte in the two phases. The most commonly used aqueous redox couples are highly charged and are therefore unlikely to partition into organic solutions under the typical conditions used in ET studies at ITIES.[4,5,9−11] Selection of a suitable redox couple for the organic phase is more challenging. Ferrocene and derivatives have been a popular choice, [4,5,12−18] but the cationic form of less hydrophobic species, such as ferrocene (Fc) and 1,1′-dimethylferrocene (DMFc), have been shown to partition extensively into water from DCE, unless a high concentration of an appropriate electrolyte is used in the aqueous phase, salting out the components of the organic electrolyte and the organic redox couple from the aqueous phase.[19,20]

It is clearly important to be able to assess the extent of partitioning of an organic redox couple across an ITIES, under the practical conditions of ET studies. Moreover, there is considerable interest in developing new methods for studying IT kinetics at the ITIES,[21−25] particularly as new theories are emerging.[26]

SECM−DPSC has been shown to be a powerful approach for measuring the kinetics of irreversible transfer across the ITIES.[27] The work described in this paper extends this approach to reversible transfer processes from both a theoretical and practical perspective. In particular, the methodology is illustrated through studies on the partitioning of the cationic form of Fc, DMFc, and decamethylferrocene (DCMFc) across the DCE/aqueous interface in the presence of ClO_4^- as a common potential-determining ion in the two phases.

SECM−DPSC Principles

The basic concepts of the SECM−DPSC approach for probing the reversible transfer of a target species across a two-phase boundary are illustrated schematically in Figure 1. A potential is applied to the UME tip positioned in one of the phases (phase 1), close to the interface of interest to generate a target species (Ox in Figure 1) by electrolysis of a precursor (Red in Figure 1) for a fixed length of time t_{sw} in an initial forward step. During this period, the tip-generated species diffuses to the interface and may transfer across it, altering the concentration

* To whom correspondence should be addressed. E-mail: P.R.Unwin@warwick.ac.uk.

10.1021/jp010591v CCC: $20.00 © 2001 American Chemical Society
Published on Web 11/06/2001

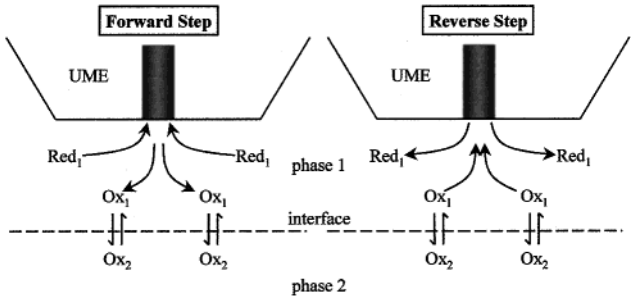

Figure 1. Schematic (not to scale) of the principles of SECM−DPSC for initiating and measuring the reversible transfer of a solute across a target interface.

profile of Ox from that expected when there is no transfer across the interface and Ox leaks out of the tip−interface gap by hindered diffusion. When a second (reverse) potential step is applied to the UME to collect back Ox, regenerating the initial species, the corresponding current−time response of the UME provides information on the interaction of Ox with the interface (partitioning in the case of the studies in this paper).

The quantitative application of SECM−DPSC to probe the partition coefficient and kinetics of the transfer of Ox across the interface requires knowledge of the tip−interface distance. If the initial precursor species, Red, is inert with respect to the interface, i.e., only soluble in phase 1, the current−time response of the UME during the forward potential step can be fitted to give an independent measure of the tip−interface separation, as discussed previously for SECM single-step[28,29] and double-potential step[27] chronoamperometry. For all the redox couples considered in this study, the solubility of the reduced species in water is negligible compared to the solubility in the organic phase.

Theory: Formulation of the Model and Numerical Solution

The diffusion of species Ox and Red in each phase is governed by the following dimensionless time-dependent diffusion equations, appropriate to the axisymmetric cylindrical geometry of the SECM.

$$\frac{\partial C_{\mathrm{Red}_1}}{\partial \tau} = \left[\frac{\partial^2 C_{\mathrm{Red}_1}}{\partial R^2} + \frac{1}{R}\frac{\partial C_{\mathrm{Red}_1}}{\partial R} + \frac{\partial^2 C_{\mathrm{Red}_1}}{\partial Z^2}\right] \tag{1}$$

$$\frac{\partial C_{\mathrm{Ox}_i}}{\partial \tau} = \gamma_{\mathrm{Ox}_i}\left[\frac{\partial^2 C_{\mathrm{Ox}_i}}{\partial R^2} + \frac{1}{R}\frac{\partial C_{\mathrm{Ox}_i}}{\partial R} + \frac{\partial^2 C_{\mathrm{Ox}_i}}{\partial Z^2}\right] \tag{2}$$

$i = 1$ for $0 \le R \le RG$, $0 < Z < L$
$i = 2$ for $0 \le R \le RG$, $Z > L$

In these equations subscript 1 or 2 on Red and Ox signifies the phase, and the dimensionless terms τ, R, and Z are given, respectively, by

$$\tau = tD_{\mathrm{Red}_1}/a^2 \tag{3}$$

$$R = r/a \tag{4}$$

$$Z = z/a \tag{5}$$

Here, the axisymmetric cylindrical coordinate system starts at the center of the UME surface with r as the radial coordinate and z the normal coordinate. The target interface is located at $Z = L$, where $L = d/a$, and extends over an infinite distance in the R direction. The parameters a and d denote the electrode radius and tip to interface distance, respectively. The normalized parameter, $RG = r_s/a$ where r_s is the radial distance between the center of the UME and the edge of the probe.

The concentrations of Red and Ox have been normalized with respect to the initial bulk concentration of Red in phase 1.

$$C_{\mathrm{Red}_1} = \frac{c_{\mathrm{Red}_1}}{c^*_{\mathrm{Red}_1}}, \quad C_{\mathrm{Ox}_i} = \frac{c_{\mathrm{Ox}_i}}{c^*_{\mathrm{Red}_1}} \qquad i = 1 \text{ or } 2 \tag{6}$$

The parameter γ_{Ox_i} is defined as

$$\gamma_{\mathrm{Ox}_i} = \frac{D_{\mathrm{Ox}_i}}{D_{\mathrm{Red}_1}} \qquad i = 1 \text{ or } 2 \tag{7}$$

It is assumed that apart from excess supporting electrolyte only a precursor species, Red_1, is initially present in phase 1 with concentration $c^*_{\mathrm{Red}_1}$ and that this species does not interact with the liquid/liquid interface. The initial conditions are thus

$$C_{\mathrm{Red}_1} = 1 \tag{8}$$

$$C_{\mathrm{Ox}_i} = 0 \tag{9}$$

$i = 1$ for $0 \le R \le RG$, $0 < Z < L$
$i = 2$ for $0 \le R \le RG$, $Z > L$

At time $\tau = 0$, the potential of the UME probe is stepped from a value where no electrode reaction occurs to one sufficient to generate the electroactive species, Ox, from the diffusion-controlled oxidation of Red.

$$\mathrm{Red}_1 - ne^- \rightarrow \mathrm{Ox}_1 \tag{10}$$

The following boundary conditions apply following this potential step and prior to the reverse step at $\tau = \tau_{sw}$:

$0 < \tau \le \tau_{sw}$, $Z = 0$, $0 \le R \le 1$:

$$C_{\mathrm{Red}_1} = 0, \quad -\gamma_{\mathrm{Ox}_1}\frac{\partial C_{\mathrm{Ox}_1}}{\partial Z} = \frac{\partial C_{\mathrm{Red}_1}}{\partial Z} \tag{11}$$

$0 < \tau \le \tau_{sw}$, $Z = 0$, $1 < R \le RG$:

$$\frac{\partial C_{\mathrm{Red}_1}}{\partial Z} = 0, \quad \frac{\partial C_{\mathrm{Ox}_1}}{\partial Z} = 0 \tag{12}$$

$0 < \tau \le \tau_{sw}$, $0 < Z < L$, $R > RG$: $C_{\mathrm{Red}_1} = 1$, $C_{\mathrm{Ox}_1} = 0$ (13)

$0 < \tau \le \tau_{sw}$, $Z > L$, $R > RG$: $C_{\mathrm{Ox}_2} = 0$ (14)

$0 < \tau \le \tau_{sw}$, $0 < Z < L$, $R = 0$: $\frac{\partial C_{\mathrm{Red}_1}}{\partial R} = 0$, $\frac{\partial C_{\mathrm{Ox}_1}}{\partial R} = 0$ (15)

$0 < \tau \le \tau_{sw}$, $Z > L$, $R = 0$: $\frac{\partial C_{\mathrm{Ox}_2}}{\partial R} = 0$ (16)

$0 < \tau \le \tau_{sw}$, $Z \rightarrow \infty$, $0 \le R \le RG$: $C_{\mathrm{Ox}_2} = 0$ (17)

$0 < \tau \le \tau_{sw}$, $Z = L$, $0 \le R \le RG$: $\frac{\partial C_{\mathrm{Red}_1}}{\partial Z} = 0$ (18)

The significance of the boundary conditions is as follows: species Red is electrolyzed at the tip at a diffusion-controlled rate (equation 11) producing Ox, but both Red and Ox are inert on the insulating glass sheath surrounding the electrode (eq 12). Equations 13 and 14 reflect the fact that the species remain at

initial bulk concentration values beyond the radial edge of the tip−substrate domain. The zero radial flux boundary conditions at $R = 0$ (eqs 15 and 16) is a consequence of the SECM axisymmetric cylindrical geometry. Equation 17 refers to the concentration of the electrogenerated species, Ox, at a semi-infinite distance from the electrode, in phase 2. Equation 18 represents the assumption that the initial precursor species, Red_1, is inert with respect to the boundary between the two phases. A further condition is imposed that describes the reversible transfer of species Ox across this interface at all times.

$$Z = L, \quad 0 \le R \le RG: \qquad -\gamma_{Ox_1}\frac{\partial C_{Ox_1}}{\partial Z} = -\gamma_{Ox_2}\frac{\partial C_{Ox_2}}{\partial Z} = K\left[C_{Ox_1} - \frac{C_{Ox_2}}{K_e}\right] \quad (19)$$

The normalized rate constant K is given by

$$K = \frac{k_1 a}{D_{Red_1}} \quad (20)$$

where k_1 is the first-order interfacial rate constant for the transfer of Ox from phase 1 to phase 2. K_e is the partition coefficient of Ox between the two phases (defined as the ratio of equilibrium concentration of species Ox in phase 2 to that in phase 1).

For this forward potential step the normalized current ratio at the UME is given by

$$\frac{i}{i(\infty)} = \left(\frac{\pi}{2}\right)\int_0^1 \left(\frac{\partial C_{Red_1}}{\partial Z}\right)_{Z=0} R\, dR \quad (21)$$

In this equation $i(\infty)$ is the steady-state diffusion-limited current for the oxidation of Red at an inlaid disk electrode positioned at an effectively infinite distance from the interface.[30]

$$i(\infty) = 4nFaD_{Red_1}c^*_{Red_1} \quad (22)$$

where n is the number of electrons transferred per redox event and F is Faraday's constant.

At time $\tau = \tau_{sw}$, the potential of the UME tip is stepped back to electrolyze species Ox to Red at a diffusion-controlled rate.

$$Ox_1 + ne^- \rightarrow Red_1 \quad (23)$$

The tip current response during this reverse step depends solely on Ox, evaluated by solving eq 2 subject to eq 19 and the following boundary conditions, having similar meanings to those outlined above

$$\tau > \tau_{sw}, \quad Z = 0, \quad 0 \le R \le 1: \quad C_{Ox_1} = 0 \quad (24)$$

$$\tau > \tau_{sw}, \quad Z = 0, \quad 1 < R \le RG: \quad \frac{\partial C_{Ox_1}}{\partial Z} = 0 \quad (25)$$

$$\tau > \tau_{sw}, \quad R = 0: \quad \frac{\partial C_{Ox_i}}{\partial R} = 0 \quad (26)$$

$$i = 1 \quad \text{for } 0 < Z < L$$
$$i = 2 \quad \text{for } Z > L$$

$$\tau > \tau_{sw}, \quad R > RG: \quad C_{Ox_i} = 0 \quad (27)$$

$$i = 1 \quad \text{for } 0 < Z < L$$
$$i = 2 \quad \text{for } Z > L$$

$$\tau > \tau_{sw}, \quad Z \rightarrow \infty, \quad 0 \le R \le RG: \quad C_{Ox_2} = 0 \quad (28)$$

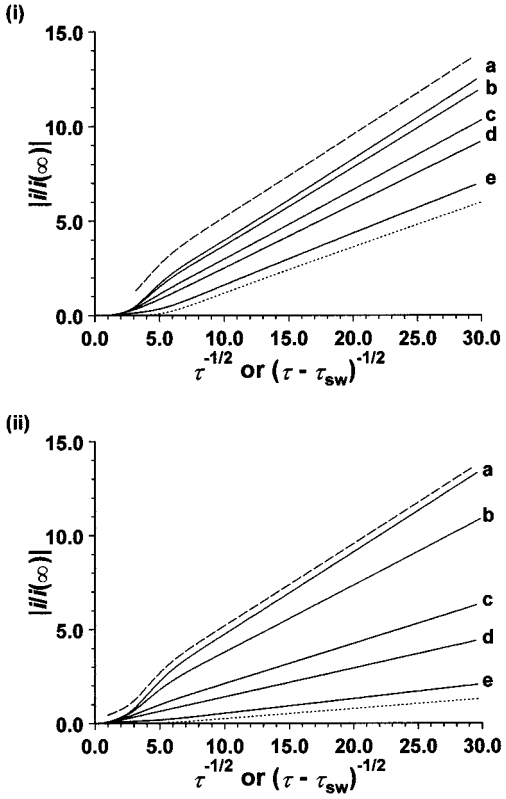

Figure 2. Forward (dashed line) and reverse (solid lines) chronoamperometric characteristics plotted as $|i/i(\infty)|$ versus $\tau^{-1/2}$ (forward step) or $(\tau - \tau_{sw})^{-1/2}$(reverse step) for $\tau_{sw} = 0.1$ (i) and 1.0 (ii). Reverse transients are for $K = 10^5$, $\gamma_{Ox_1} = \gamma_{Ox_2} = 1$, and $K_e = 0$ (a), 0.1 (b), 0.5 (d), 1.0 (d), and 5.0 (e). The dotted line in each case is the reverse characteristic for irreversible transfer kinetics with $K = 10^5$.

The corresponding current ratio for the reverse potential step is given by

$$\frac{i}{i(\infty)} = -\gamma_{Ox_1}\left(\frac{\pi}{2}\right)\int_0^1 \left(\frac{\partial C_{Ox_1}}{\partial Z}\right)_{Z=0} R\, dR \quad (29)$$

The problem was solved numerically using a FORTRAN program based on the alternating direction implicit finite difference algorithm,[31,32] which has found widespread application in the treatment of SECM problems.[27,33−35] The finite difference grid employed was similar to that described for recent two-phase problems.[34]

Theoretical Results and Discussion

The normalized SECM−DPSC response depends on the parameters L, K, K_e, γ_{Ox_1}, γ_{Ox_2}, τ and τ_{sw}. If the long time behavior is considered, the value of RG is also important. The main aim in this section is to give a general appraisal of the influence of K_e and K on the DPSC characteristics compared to the previously reported model,[27] which considered only irreversible transfer kinetics. To limit the length of the discussion, theoretical results are presented for the general case where $RG = 10$, $\gamma_{Ox_1} = \gamma_{Ox_2} = 1$, and for a normalized tip−interface separation of $\log(L) = -0.5$, which is typical of the close distances to the ITIES that are readily achievable in the SECM−DPSC experiments reported in this paper.

The effect on the current−time response of varying K_e under conditions where the kinetics of the interfacial transfer are fast and nonlimiting is shown in Figure 2, for two switching times,

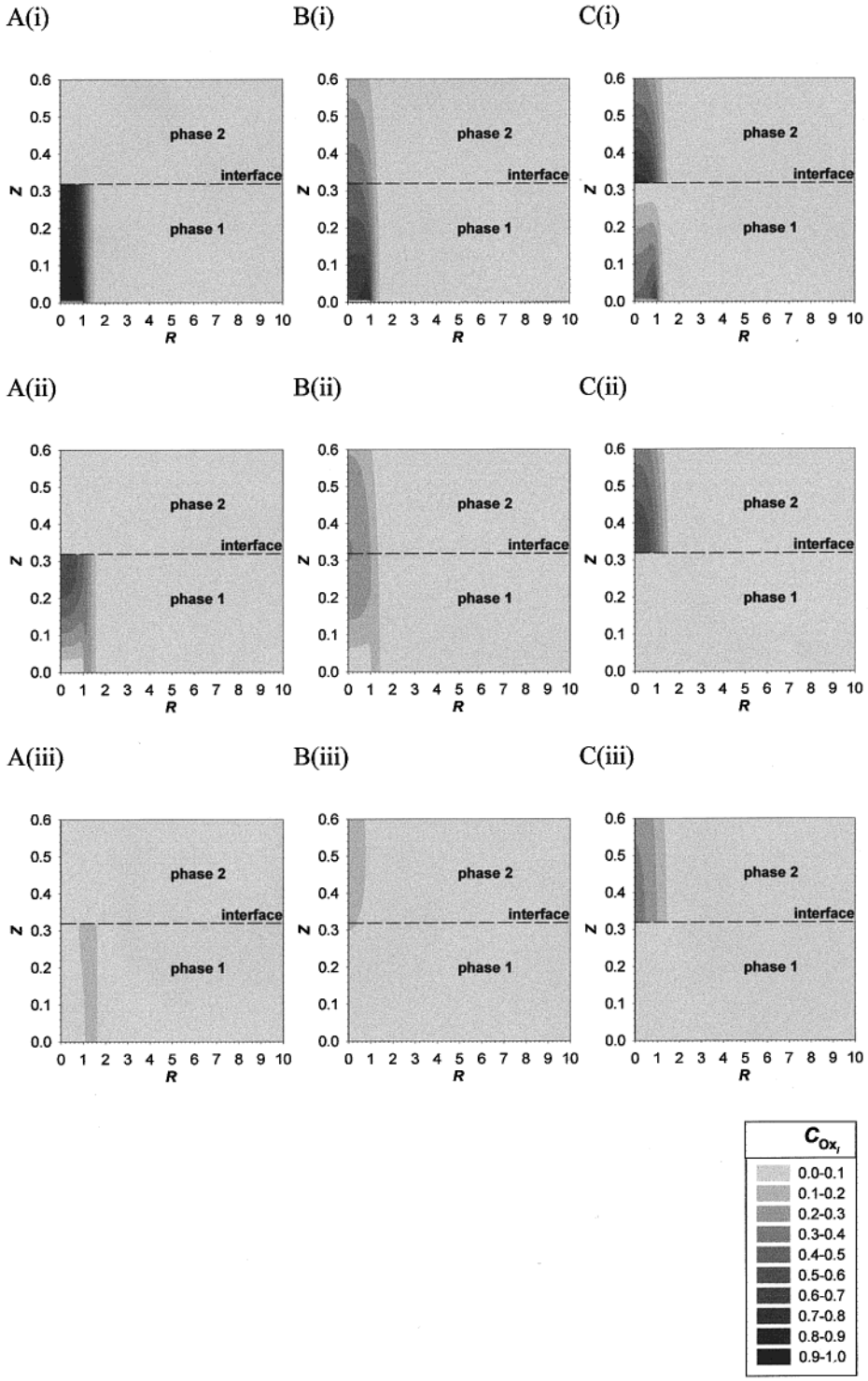

Figure 3. Evolution of the concentration profile of Ox during the reverse potential step. Data are shown for $\tau_{sw} = 0.1$ and $K_e = 0.01$ (A), 1.0 (B), and 100 (C) immediately after the potential is reversed (i) and at $(\tau - \tau_{sw}) = 0.025$ (ii) and 0.1 (iii).

$\tau_{sw} = 0.1$ (Figure 2i) and 1.0 (Figure 2ii). For the range of K_e values of interest, a value of $K = 10^5$ was sufficient to ensure that interfacial kinetics were effectively nonlimiting for the switching times examined, for this particular tip−interface separation. These plots show $|i/i(\infty)|$ versus $\tau^{-1/2}$ or $(\tau - \tau_{sw})^{-1/2}$ for the forward and reverse steps, respectively, thereby emphasizing the short time characteristics of the UME response. For a constant τ_{sw} the forward transients are the same, irrespective of the value of K_e or K, since during the forward step the current response is governed by the hindered diffusion of the initial precursor species, Red, to the tip, which is inert toward the interface. The form of the transient response for an UME positioned close to an inert interface has been discussed previously for SECM single-[28,29] and double-potential-step[27] chronoamperometry. In brief, at short times, for which the extent of the diffusion layer at the UME is small compared to the tip−interface distance, the transient response is identical to that expected for an UME in bulk solution. At longer times, sufficient for the diffusion field to have intercepted the interface ($\tau^{-1/2} \approx 1/L$), diffusion of Red toward the probe is hindered and the current flowing at the tip is lower than for an UME in bulk solution at the same time.

By comparison, the transient response during the reverse potential step shows a strong dependence on K_e, particularly at the longer switching time. For a low K_e value, $K_e = 0.1$, the extent of transfer across the interface is small during the forward potential step and Ox is impeded from diffusing out of the gap between the probe and the interface by the presence of the interface. The current flowing immediately after the potential is reversed is high but then decreases rapidly as Ox is extensively depleted within the tip−interface region. In this case, as expected, the reverse chronoamperometric response only deviates slightly from that predicted for an interface that is inert to both Red and Ox, calculated by either setting $K = 0$ in the numerical model outlined above, or using the inert interface model reported elsewhere.[27] Deviation from the inert interface model increases for longer τ_{sw}, indicating that the DPSC response is most sensitive to low K_e at long τ_{sw}.

As K_e is increased the reverse currents are diminished for the two switching times considered in Figure 2. A higher value of K_e corresponds to an increased tendency of Ox to transfer across the interface from phase 1 to phase 2. The transfer acts as a reversible, partial sink for the extraction of species Ox from the tip−interface gap. As a consequence, smaller currents result when the potential is reversed in a stepwise fashion. This effect is evident in the typical concentration profiles of Ox for $\tau_{sw} = 0.1$ (Figure 3). The profiles immediately after the potential step is reversed show that, as K_e increases the partitioning of Ox into phase 2 increases which affects the subsequent diffusion profiles and current−time behavior. Additional concentration profiles considered elsewhere[36] demonstrate that depletion of Ox in phase 1 becomes more prevalent as τ_{sw} is increased, as expected. For all switching times examined, the reverse chronoamperometric response for $K_e \geq 100$ was found to be indistinguishable from that predicted using the earlier model for irreversible transfer with $K = 10^5$.[27]

The results in Figure 2 demonstrate that, under the defined conditions, for practical switching times, the reverse DPSC response is sensitive to K_e over a wide range, from a lower limit of less than 0.1 to an upper limit greater than 5.0. It is also apparent from Figure 2 that a longer switching time offers the best resolution of processes characterized by a value of K_e at the lower limit of this range, whereas a shorter switching time is most useful for processes characterized by larger K_e.

The effect of interfacial kinetic limitations on the reverse DPSC response has been described extensively for $K_e \rightarrow \infty$[27] and is considered briefly in Figure 4 for a finite value of $K_e = 1$. For low values of K, the response of the interfacial equilibrium is slow compared to the flux of Ox generated at the electrode and hence the concentration of Ox builds up in the tip−interface gap (phase 1). The current flowing at all times following the reverse potential step therefore increases as K decreases and the transient response approaches that predicted for an interface that is inert with respect to Ox. Conversely, for large K an upper limit is reached where the interfacial kinetics are sufficiently fast, on the time scale of the DPSC measurement, that the chronoamperometric behavior is governed by the rate of mass transfer of Red and Ox in the two phases during the forward and reverse steps. The effect of finite kinetics on the measurement of K_e is that the consequent diminution in the extent of Ox transfer across the interface makes the DPSC response less sensitive to the K_e value, particularly at the shortest switching times.

In common with other SECM kinetic applications, the effective time scale of DPSC measurements can be altered by varying the size of the probe and the probe-interface distance.

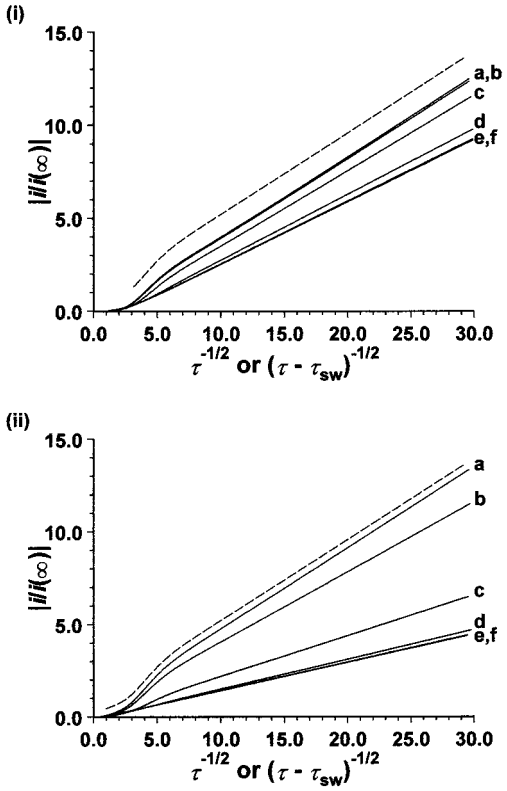

Figure 4. Forward (dashed line) and reverse (solid lines) chronoamperometric characteristics plotted as $|i/i(\infty)|$ versus $\tau^{-1/2}$ (forward step) or $(\tau - \tau_{sw})^{-1/2}$(reverse step) for $\tau_{sw} = 0.1$ (i) and 1.0 (ii). Reverse transients are for $K_e = 1$ and $K = 0$ (a), 0.1 (b), 1.0 (c), 10 (d), 100 (e), and 1000 (f).

An additional attribute of SECM−DPSC is that the switching time can be controlled to optimize the sensitivity of the response to the kinetic region of interest. This aspect is manifest in the data in Figure 4 where the response for the shortest switching time is most sensitive to fast interfacial kinetics, whereas the response for the longest switching time is most sensitive to slower interfacial processes. For typical values of $D_{Red_1} = D_{Ox_1} = D_{Ox_2} = 1.0 \times 10^{-5}$ cm^2 s^{-1} and an electrode radius of $a = 12.5$ μm, with the remaining conditions as defined for Figure 4, it should be possible to measure first-order heterogeneous rate constants in the range $k_1 = 0.0008-0.8$ cm s^{-1}, using a switching time, $t_{sw} = 0.016$ s.

The theoretical results presented above have practical implications for the independent measurement of the partition coefficient and rate constant characterizing the fast reversible transfer of a target species across an interface between two immiscible phases. This is a consequence of the different sensitivity of the SECM−DPSC response to K_e and K for different switching times. For long switching times, compared to the time scale of the interfacial transfer process, the concentrations of the target species adjacent to the interface are essentially close to equilibrium and the reverse DPSC response will depend on K_e but will be insensitive to K. Once K_e is known, the rate constant for the transfer may be targeted by employing a short switching time, which is most sensitive to fast kinetics. This strategy is adopted in the experimental studies reported in this paper.

Experimental Section

Chemicals and Materials. All chemicals were used as received. Ferrocene (Fc, 98%), 1,1′-dimethylferrocene (DMFc, 97%), bis(pentamethylcyclopentadienyl) iron (DCMFc, 97%),

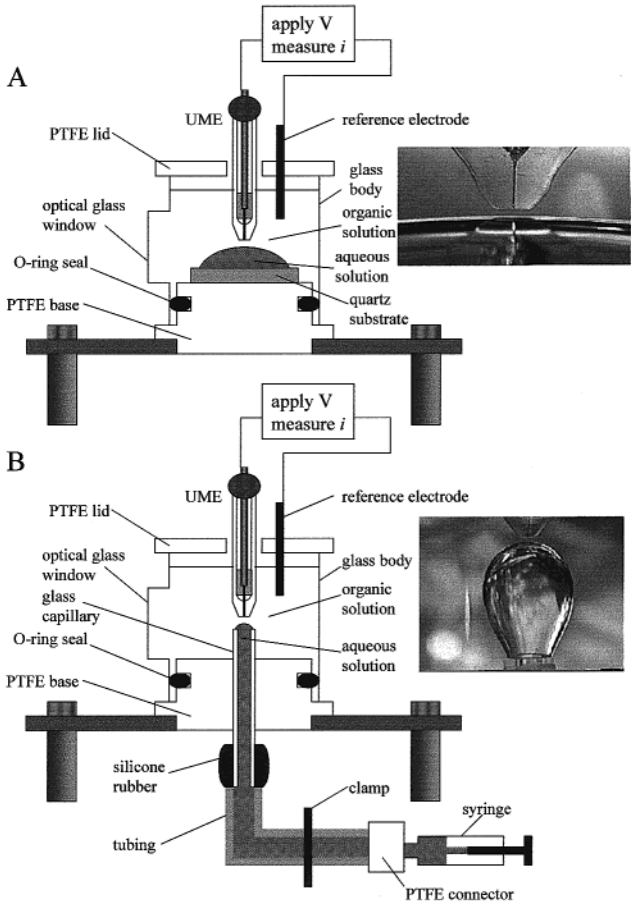

Figure 5. Examples of the setups used in studies of the partitioning of the oxidized form of the ferrocene species across the DCE/aqueous interface.

ferrocenium hexafluorophosphate ($FcPF_6$), DCE (HPLC grade), $LiClO_4$ (+95%), $NaClO_4 \cdot xH_2O$ (A. R.), and tetrabutylammonium perchlorate (TBAP) were all obtained from Sigma-Aldrich (Gillingham, UK). Other chemicals were NaCl (A. R., Fisons, Loughborough, UK) and tetra-*N*-hexylammonium perchlorate (THAP, Alfa Aesar, Karlsruhe, Germany). Aqueous solutions were made using 18 MΩ cm water (Milli-Q reagent water, Millipore Corp.) and typically contained 0.025−1 M $LiClO_4$ (for exceptions see below). DCE solutions were generally prepared with 2−10 mM of the ferrocene mediator and 0.1−0.25 M TBAP or THAP as supporting electrolyte. To deaerate solutions, nitrogen (white spot, BOC) was bubbled through (for details see below).

Instrumentation and Methods. General details on the instrumentation for SECM transient measurements have been reported in full elsewhere.[11,27,34,36] SECM−DPSC studies employed a 25 μm diameter disk-shaped Pt UME as the working electrode and a silver quasi reference electrode (AgQRE). Both electrodes were positioned in the DCE phase. The potential of the UME was first jumped to a value where oxidation of Fc to Fc^+ was diffusion-controlled and then, after a defined period, back to a potential to collect Fc^+ by diffusion-controlled reduction. The potentials were determined from the steady-state voltammetric response of the UME in bulk DCE.

For investigations of the partitioning of the oxidized ferrocene derivatives between DCE and water, the methodology adopted was similar to that advocated by Shao et al.[37] This involved placing the denser organic phase on top of the aqueous phase, to enable a conventional UME and SECM apparatus to be used. Two setups were considered, as shown in Figure 5. In the setup in Figure 5A, the liquid/liquid interface was formed between a drop of aqueous solution supported on a clean quartz substrate and an overlying DCE solution. The drop diameter was approximately 15 mm, so that the region of the ITIES probed by the UME was effectively flat on the SECM scale. In the second setup, Figure 5B, an aqueous drop was formed at the end of a borosilicate glass capillary, by flowing the aqueous solution through it using a 500 μL gastight syringe (Hamilton, Reno, NA). The advantage of the latter approach was that the interface was readily renewable.

A twin electrode thin layer cell (TLC) was used to investigate the stability of electrogenerated Fc^+. A four-electrode arrangement was employed, using an Oxford Electrodes (Oxford, UK) bipotentiostat, modified in house to include an option allowing currents to be measured with gains of $10^{-6}-10^{-9}$ A V^{-1} as well as the conventional $10^{-3}-10^{-6}$ A V^{-1} range. A AgQRE and a Pt gauze auxiliary electrode were employed. The two working electrodes (one generating Fc^+ by oxidation of Fc and one collecting Fc^+ by reduction) were 1.6 mm diameter Pt disk electrodes (MF-2013, BAS). A conventional two-piece electrochemical cell was used with the PTFE base modified to accommodate one of the Pt disk electrodes. The other electrode was held in a home-built device attached to the piezoelectric positioner of the SECM instrument.[11,17,34,36] The disk electrodes were aligned using *x*, *y*, *z* manual positioners with the aid of video zoom microscopy.

All electrochemical measurements were made at ambient temperature, which was measured and was generally 21−22 °C, unless otherwise stated. Some of the consequences of working at slightly higher temperature are considered later in this paper.

The solubility of $FcPF_6$ in aqueous solutions of 0.1 M $LiClO_4$ was investigated as a function of temperature by UV−vis spectrophotometry, using a 1 cm path length, 4 mL volume quartz cuvette. Absorbances were recorded at the wavelength of maximum absorbance, $\lambda = 252$ nm using an UV/visible spectrometer (Unicam, model 8625). The absorbance of solutions containing $FcPF_6$ over the concentration range of interest and 0.1 M $LiClO_4$ was measured, to check for Beer−Lambert characteristics and to determine extinction coefficients. To measure the concentration of Fc^+ in saturated solutions at different temperatures, a generous excess of $FcPF_6$ (0.166 g) was added to a volumetric flask, placed in a thermostated water bath, containing 10 mL of the aqueous solution, that had been purged with N_2 for 40 min. The solution was agitated for 1 h, by bubbling through N_2, and the degassing line was then removed from the solution and N_2 was blown over the top of the solution to exclude air, for a further 30 min, to allow the undissolved solid to settle. An aliquot of the saturated solution was then removed and immediately diluted in 240 parts of 0.1 M $LiClO_4$ solution, which was maintained at the same temperature.

Experimental Results and Discussion

Fc/Fc^+ Voltammetry. The oxidation of Fc and derivatives is considered to be a fast reversible one-electron process for a variety of solvents and electrodes.[38−41] Steady-state linear sweep voltammetric measurements (scan rate ≥ 5 mV s^{-1}) of the oxidation of 2.2 mM Fc in an aerated DCE solution containing 0.1 M TBAP resulted in separations between the half-wave and quarter-wave potentials, $\Delta E_{1/4} = E_{1/2} - E_{1/4} = 29$ (± 0.5) mV and the three-quarter-wave and half-wave potentials, $\Delta E_{3/4} = E_{3/4} - E_{1/2} = 28$ (± 0.5) mV at 23 °C indicating that the ET exhibited near Nernstian behavior.[42,43] The limiting steady-state

plateau current was 11.0 (± 0.2) nA, giving $D_{Fc} = 1.04 (\pm 0.02) \times 10^{-5}$ cm^2 s^{-1}, which is a reasonable value based on the size of the Fc molecule.[44] The oxidation of DMFc and DCMFc in DCE were also found to be close to reversible on the time scale of UME steady-state linear sweep voltammetry with values for the diffusion coefficients, $D_{DMFc} = 9.64 (\pm 0.2) \times 10^{-6}$ cm^2 s^{-1} and $D_{DCMFc} = 7.4 (\pm 0.35) \times 10^{-6}$ cm^2 s^{-1}.

Assessment of the Stability of Fc^+. To make SECM−DPSC measurements with the highest precision, it was important to consider the stability of the electrogenerated Fc^+ ion on the SECM time scale. There have been reports of complications associated with the heterogeneous electrochemical oxidation of Fc in organic solvents, including possible reactant/product adsorption processes[39] and formation of passivating films on electrodes.[45−47] Film formation has been linked to the decomposition of Fc^+ forming insoluble products that foul the electrode. There is evidence for the decomposition of Fc^+ and $DMFc^+$ in the presence of dioxygen.[48,49] and the rate of decomposition of Fc^+ appears to depend on both the nature of the organic solvent[50,51] and the supporting electrolyte.[4] First-order decomposition rate constants in solutions containing 0.05 M tetrabutylammonium tetraphenylborate (TBATPB) have been measured using a Pt rotating disk electrode in nitrobenzene ($k = 0.0255$ s^{-1})[52] and DCE ($k = 0.346$ s^{-1})[5] Conversely solutions of a $DCMFc^+$ salt in air-saturated acetonitrile were found to be stable for several years.[49]

To assess the importance of Fc^+ decomposition in aerated DCE solutions, we carried out a series of simple measurements. We found that when 0.017 g of $FcPF_6$ was added to 10 cm^3 of air-saturated DCE, the initial blue solution formed changed color to dark blue/green within ~30 s and over a further 4−10 min formed a yellow/green solution and rust brown precipitate. In contrast, in water the decomposition reaction occurred much less rapidly.

In view of the apparent decomposition of Fc^+ in aerated DCE solutions, it was important to establish more precisely whether this process was significant on the time scale of the chronoamperometric measurements employed in the work described below. This was particularly pertinent since employing aerated solutions considerably simplified the practical procedure for investigating the partitioning of Fc^+ across the DCE/aqueous interface.

Attempts were made to follow the decomposition reaction amperometrically using a twin electrode TLC configuration. This technique is generally applicable for investigating the rate of chemical reactions following ET, provided the reaction half-life is sufficiently large. In particular, the approach is most simply applied when mass transfer in the thin layer is non limiting.[53−55] Two aligned, parallel Pt disk electrodes were brought into close proximity (<50 μm) in an electrochemical cell containing a solution of 0.5 mM Fc, 0.1 M TBAP in DCE, so that a thin layer of the solution was trapped between the electrodes. The potential of one of the electrodes (generator) was stepped from 0 V, where no electrode processes occurred, to +0.7 V versus AgQRE, where the generation of Fc^+, from the oxidation of Fc, occurred at a diffusion-controlled rate, while the potential of the second electrode (collector) was held at −0.2 V to effect the diffusion-controlled reconversion of Fc^+ back to Fc. In this way, a feedback cycle of Fc/Fc^+ was established in the thin layer of solution between the electrodes.

Figure 6 shows examples of the chronoamperometric responses of the generator and collector electrodes, following the potential step, when the DCE solution was either aerated or had been purged with Ar for ca. 30 min. The separation between

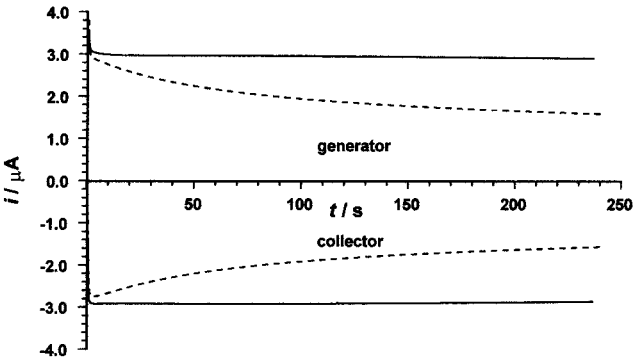

Figure 6. Current−time characteristics of 1.6 mm diameter Pt disk electrodes, in a twin electrode TLC arrangement, for a DCE solution containing 0.5 mM Fc and 0.1 M TBAP, when the solution was thoroughly deaerated (solid lines) and aerated (dashed lines). The generator electrode was stepped from 0.0 to 0.7 V (versus AgQRE) to effect the oxidation of Fc at a diffusion-controlled rate and the collector electrode was held at −0.2 V to convert Fc^+ back to Fc.

the two electrodes, measured as 30 ± 2.5 μm using a video microscope, was the same in both cases. For the deaerated solution, the transient responses of the generator and collector electrodes quickly reach the same, steady-state current, which is as expected in the absence of coupled reactions.[53] The diffusion-limited steady-state current for simple electron transfer in a twin electrode TLC is given by[53]

$$i_d = \frac{2nFAc^*}{l}\frac{D_O D_R}{D_O + D_R} \qquad (30)$$

where A is the area of the electrodes, l is the thickness of the thin layer, c^* is the sum of the concentrations of the oxidized and reduced species (averaged from 0 to l) and D_O and D_R are, respectively, the diffusion coefficients of the oxidized and reduced forms of the redox couple. Using the measured value of $i_d = 2.96$ μA, $A = 0.0201$ cm^2, $c^* = 0.5$ mM, $D_{Fc,DCE} = 1.05 \times 10^{-5}$ cm^2 s^{-1}, and $D_{Fc^+,DCE} = 6.8 \times 10^{-6}$ cm^2 s^{-1}, measured by UME chronoamperometry in bulk solution,[36,56] as highlighted later, eq 30 gives $l = 27$ μm for these data.

In contrast, the transient responses for the aerated solution show a pronounced decay in the current with increasing time, as found when there is a following chemical reaction.[53−55] It was not possible to analyze the data as a simple first- or second-order process, possibly because the decay in the current is not only due to a loss of Fc^+ in solution, but also due to passivation of the electrodes, as discussed above.

The occurrence of the film formation side reactions is expected to be less prevalent for ultramicroelectrodes than for confined macrosized electrodes, owing to the more rapid rates of mass transport which characterize the micrometer-sized electrodes. This is borne out in the linear sweep voltammetric results described above. These results agree with previous investigations of Fc oxidation in acetonitrile solutions, which found that film formation on Pt UMEs (1−25 μm diameter) was insignificant for dilute solutions (<10 mM Fc) on the time scale of steady-state UME voltammetry.[57,58]

Determination of Diffusion Coefficients via DPSC in Bulk Solution. When employed in bulk solution, DPSC at UMEs provides valuable information on the diffusion coefficients of both the oxidized and reduced forms of a stable couple.[27,56] This approach has previously been used to determine the diffusion coefficients of the reduced and oxidized forms of the ferrocene redox couples in aerated solutions of DCE, which are required to implement the SECM−DPSC approach quantitatively.[59]

Typical measured values in DCE solutions containing 0.1 M TBAP were as follows: $D_{Fc,DCE} = (1.04 \pm 0.03) \times 10^{-5}$ cm^2 s^{-1}, $D_{Fc^+,DCE} = (7.0 \pm 0.5) \times 10^{-6}$ cm^2 s^{-1}, $D_{DMFc,DCE} = (9.45 \pm 0.05) \times 10^{-6}$ cm^2 s^{-1}, $D_{DMFc^+,DCE} = (6.0 \pm 0.2) \times 10^{-6}$ cm^2 s^{-1}, $D_{DCMFc,DCE} = (7.75 \pm 0.05) \times 10^{-6}$ cm^2 s^{-1}, and $D_{DMFc^+,DCE} = (6.35 \pm 0.25) \times 10^{-6}$ cm^2 s^{-1}.There was no significant change in the measured values of $D_{Fc,DCE}$ or $D_{Fc^+,DCE}$, using switching times up to 0.400 s, when the organic solution was deaerated thoroughly by bubbling N_2 through the solution for at least 40 min. These results indicate that decomposition of Fc^+ in the presence of O_2 was negligible on the time scale of these DPSC measurements.

The diffusion coefficient of Fc^+ in aqueous solution was estimated from single potential step chronoamperometry measurements for a solution of ferrocenium hexafluorophosphate, $FcPF_6$. Because of the low solubility of Fc in water (of the order of 10^{-5} M)[38,39,46,60] it was necessary to use a low concentration of the Fc^+ salt ($\sim$1 mM) and a short transient duration ($\sim$0.45 s) to avoid possible complications from the adsorption or precipitation of Fc. Measurements made with 0.1 M $LiClO_4$ as supporting electrolyte gave a value of $D_{Fc^+,aq} = (6.6 \pm 0.3) \times 10^{-6}$ cm^2 s^{-1}, which is significantly higher than the values previously obtained for aqueous solutions containing 0.01 M Li_2SO_4 ($D_{Fc^+,aq} = 1.7 \times 10^{-6}$ cm^2 s^{-1}) or 1.5 M Li_2SO_4 ($D_{Fc^+,aq} = 2.1 \times 10^{-7}$ cm^2 s^{-1}).[4]

SECM−DPSC Studies of the Partitioning of Fc^+ across the DCE/Aqueous Interface. To investigate the extent of partitioning of Fc^+ across the DCE/aqueous interface, DPSC measurements were made with the probe UME positioned close to the interface between DCE and an aqueous drop. In these experiments, Fc^+ was generated at the tip from the oxidation of Fc in DCE in an initial potential step from 0.0 to 0.7 V, for a period in the range 0.01−0.4 s. After this time the potential of the tip was stepped from 0.7 V to −0.2 V to collect Fc^+.

The presence of ClO_4^- as the common supporting ion in the two phases served two functions: as a potential-determining ion to poise the initial potential across the interface and to transfer commensurately with Fc^+ to maintain charge neutrality. It should be noted that the local potential across the ITIES in the region directly under the electrode may vary during the course of an SECM measurement.[61] To minimize this effect, experiments were carried out with the concentration of ClO_4^- ions in relatively high excess. The coupled transfer of Fc^+ and ClO_4^- across the ITIES essentially parallels the dissolution of a salt from DCE into the aqueous phase. It was anticipated and confirmed (vide infra) by these experiments that the transfer process would by fairly rapid ($k_1 > 0.1$ cm s^{-1}). Previous work by our group suggested that Fc^+ and $DCMFc^+$ form strong ion pairs with ClO_4^- in DCE.[11] An important point concerns whether the partitioning of the ferricinium species across the ITIES involves transfer of the individual ions, transfer as an ion pair or a mixed process. Although the net results of these processes are identical (i.e. Fc^+ and ClO_4^- cross the ITIES), kinetically they should be different, e.g., the transfer of an ion pair is potential independent.

Figure 7 shows typical DPSC transients for the generation and collection of Fc^+ when the aqueous phase contained 0.1 M $LiClO_4$ and the DCE solution contained 5 mM Fc and 0.1 M TBAP, for a switching time, $t_{sw} = 0.374$ s. The kinetics of transfer of Fc^+ across the interface was expected, and confirmed, to be nonlimiting on the relatively long time scale of these measurements. Using the values of $D_{Fc,DCE}$ and $D_{Fc^+,DCE}$, deduced from the DPSC response with the UME positioned far from the interface, in the bulk organic solution, the forward

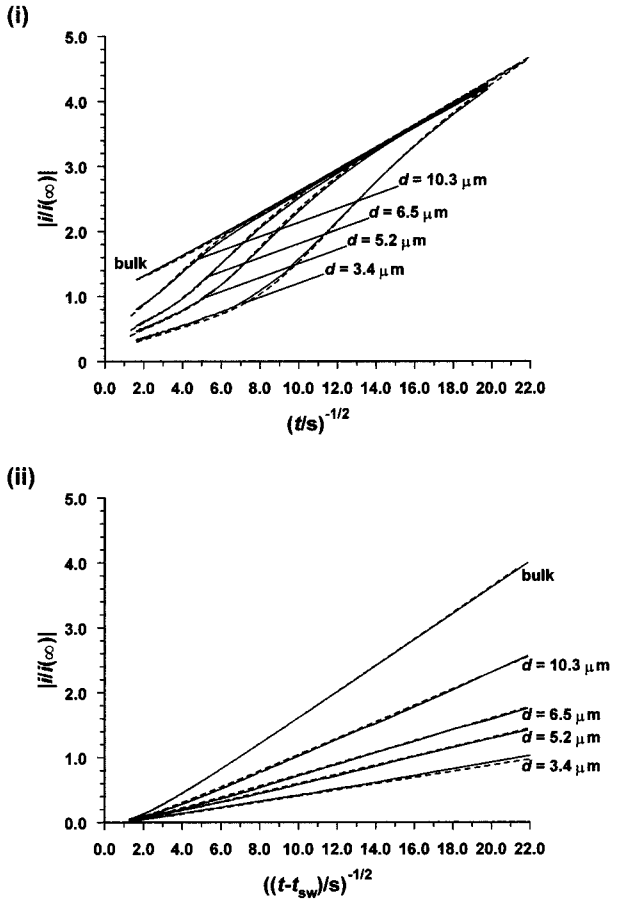

Figure 7. Typical experimental SECM−DPSC data ($t_{sw} = 0.374$ s, solid curves) for (i) the oxidation of Fc (forward step) and (ii) reduction of Fc^+ (reverse step), at a 25 μm diameter UME in a DCE solution containing 5 mM Fc and 0.1 M TBAP. The UME was located at various distances from an aqueous phase, containing 0.1 M $LiClO_4$, and in bulk DCE. The dashed curves are the theoretical DPSC characteristics for $D_{Fc,DCE} = 1.07 \times 10^{-5}$ cm^2 s^{-1} and $D_{Fc^+,DCE} = 7.5 \times 10^{-6}$ cm^2 s^{-1} (as measured from the bulk response). The best fit to the reverse DPSC transients was obtained by considering no kinetic limitations, with $D_{Fc^+,aq} = 6.6 \times 10^{-6}$ cm^2 s^{-1} and $K_e = 1.1$, at each of the tip−interface distances.

DPSC response was fitted to the theoretical behavior assuming the interface was inert toward Fc, using the tip−interface distance as the only variable. The good agreement between the experimental and theoretical data for the forward step in Figure 7i verifies that there is negligible partitioning of Fc into the aqueous phase. Armed with knowledge of the tip−interface separation from fitting the forward transient, the reverse response was compared to simulations using the theoretical model outlined earlier for different values of K_e. The best fit to the experimental data of Figure 7(ii) was obtained with $K_e = 1.1$ for all the tip−interface distances examined. The mean value of K_e from several separate experiments was $K_e = 1.1 \pm 0.1$.

To probe the kinetics of the transfer of Fc^+ from DCE to the aqueous phase, shorter switching times were employed. Figure 8 shows typical SECM−DPSC data for the shortest switching time examined, $t_{sw} = 0.0097$ s, at $d = 3.4$ μm. Even at this switching time, the reverse response is in good agreement with the theory for a diffusion-controlled interfacial transfer process. However, based on the data in Figure 8 a lower limit of $k_1 > 0.5$ cm s^{-1} can be assigned to the interfacial rate constant for the transfer process. Since the transfer kinetics are so fast on the SECM time scale, we were unable to distinguish between the various ion transfer scenarios highlighted above, although

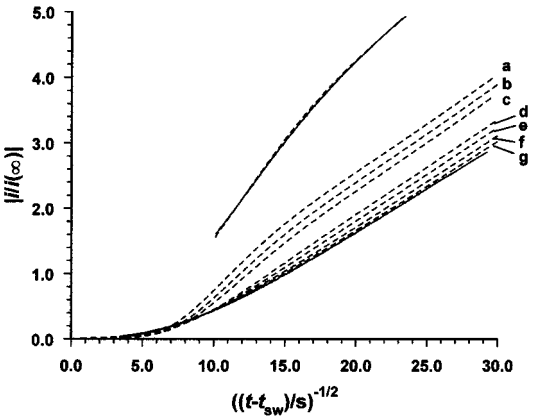

Figure 8. Typical SECM−DPSC experimental data ($t_{sw} = 0.0097$ s) for the oxidation of Fc in DCE (forward step, upper solid curve) and reduction of Fc^+ (reverse step, lower solid curve), at a 25 μm diameter UME, located in a DCE solution containing 5 mM Fc and 0.1 M TBAP, at a distance of 3.4 μm from an aqueous phase containing 0.1 M $LiClO_4$. The dashed curves are the theoretical DPSC characteristics for the forward step (upper dashed curve) and the reverse step for $D_{Fc,DCE} = 1.07 \times 10^{-5}$ cm^2 s^{-1}, $D_{Fc^+,DCE} = 7.5 \times 10^{-6}$ cm^2 s^{-1}, $D_{Fc^+,aq} = 6.6 \times 10^{-6}$ cm^2 s^{-1}, $K_e = 1.1$, and k_1/cm s^{-1} = 0.001 (a), 0.005 (b), 0.01 (c), 0.05 (d), 0.1 (e), 0.5 (f), and 10^5 (g). The timescale for the forward step is $(t/s)^{-1/2}$.

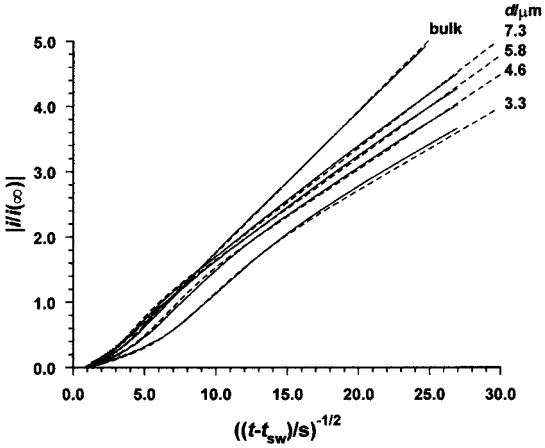

Figure 9. Typical reverse SECM−DPSC transients ($t_{sw} = 0.387$ s) for the reduction of electrogenerated $DMFc^+$ (reverse step, solid curves), at a 25 μm diameter UME, in a DCE solution containing 5 mM DMFc and 0.1 M TBAP, located at various distances from an aqueous phase containing 0.1 M $LiClO_4$ and in bulk DCE. The dashed curves are the theoretical DPSC characteristics for $D_{DMFc,DCE} = 9.45 \times 10^{-6}$ cm^2 s^{-1} and $D_{Fc^+,DCE} = 6.05 \times 10^{-6}$ cm^2 s^{-1} (as measured from the bulk response). The best fit to the reverse DPSC transients was obtained by considering no kinetic limitations, with $D_{DMFc^+,aq} = 5.32 \times 10^{-6}$ cm^2 s^{-1} and $K_e = 0.17$, at each of the tip−interface distances (determined from the DPSC transient during the forward step).

ion-pair transfer is the most likely candidate given the strong ion pair formation already identified.

The influence of changing the ratio of $[ClO_4^-]$ in the two phases on the value of K_e and the transfer kinetics of Fc^+ was also investigated. Table 1 summarizes the measured values of K_e obtained from a series of experiments using various concentrations of ClO_4^- in each phase with a switching time $\sim$ 0.370 s. For the range of $[ClO_4^-]$ ratios shown in Table 1 the reverse DPSC behavior was indistinguishable from that expected for diffusion-controlled transfer, deduced from separate measurements with t_{sw} down to $\sim$ 0.01 s.

The distribution coefficient of ferrocenium perchlorate between the two phases is given by

$$K_d = \frac{f_{Fc^+,aq} f_{ClO_4^-,aq} [Fc^+]_{aq} [ClO_4^-]_{aq}}{f_{Fc^+,DCE} f_{ClO_4^-,DCE} [Fc^+]_{DCE} [ClO_4^-]_{DCE}} \qquad (31)$$

where f are activity coefficients for the ions of interest in the two phases. It follows that

$$K_e = K_d \frac{[ClO_4^-]_{DCE}}{[ClO_4^-]_{aq}} \frac{f_{Fc^+,DCE} f_{ClO_4^-,DCE}}{f_{Fc^+,aq} f_{ClO_4^-,aq}} \qquad (32)$$

One would thus expect K_e to increase with the ratio $\{[ClO_4^-]_{DCE}\}/\{[ClO_4^-]_{aq}\}$. This is observed, but the effect is not quantitative, which can be attributed to changes in the activity coefficient of the ions as the ionic strength varies. For example, over the concentration range of interest, as the ionic strength of the aqueous phase and thus $[ClO_4^-]_{aq}$ increases, there is likely to be a concomitant decrease in $f_{Fc^+,aq}$ and $f_{ClO_4^-,aq}$. Unfortunately, there is little reliable information on activity coefficients of ions in organic solutions and there are considerable complications from ion pair formation. Even in aqueous solution, the estimation of activity coefficients in concentrated electrolyte solutions involves some uncertainty, making further analysis of these data difficult. SECM−DPSC does however allow us to probe salt partition coefficients in a reliable and robust manner.

SECM−DPSC Studies of the Partitioning of $DMFc^+$ and $DCMFc^+$ across the DCE/Aqueous Interface. A similar experimental protocol to that described in the preceding section was used to assess whether $DMFc^+$ and $DCMFc^+$ partitioned across the DCE/aqueous interface. Figure 9 shows typical reverse step SECM−DPSC characteristics for the collection of $DMFc^+$ at an UME positioned close to the ITIES, for $t_{sw} = 0.387$ s. For these data, the DCE solution contained 5 mM DMFc and 0.1 M TBAP and the aqueous solution contained 0.1 M $LiClO_4$. The relative collection (reverse step) currents are much larger than for Fc/Fc^+ (Figure 7) indicating that the partition coefficient of $DMFc^+$ is much lower. In fact, the best fit of the reverse transient to the theoretical model was achieved for a value of $K_e = 0.17$, assuming the ratio $\{D_{DMFc^+,aq}\}/\{D_{DMFc^+,DCE}\} = 0.88$, as was found for Fc. The lower value of K_e for $DMFc^+$ compared to that obtained for Fc^+ transfer, under similar conditions, is consistent with the more hydrophobic character of the $DMFc^+$ molecule. The kinetics of the partitioning of $DMFc^+$ across the ITIES was probed using a switching time, $t_{sw} = 0.0097$ s. Due to the lower partition coefficient of $DMFc^+$ it was difficult to make accurate kinetic measurements, but the DPSC response on this time scale was again indistinguishable from the behavior predicted for a diffusion-controlled process.

To investigate whether $DCMFc^+$ partitioned across the DCE/aqueous interface, DPSC characteristics were examined for a

TABLE 1: Values of K_e as a Function of Electrolyte Concentration in the Two Liquid Phases

$[Fc]_{DCE}$/mM	supporting electrolyte in DCE phase	supporting electrolyte in aqueous phase	t_{sw}/s	K_e
5−10	0.1 M TBAP	0.1 M $LiClO_4$	0.374−0.378	1.1 ± 0.1
5	0.1 M TBAP	1.0 M $LiClO_4$	0.378	0.55 ± 0 0.05
5	0.25 M TBAP	0.05 M $LiClO_4$	0.378	1.6 ± 0.2
2	0.25 M TBAP	0.025 M $LiClO_4$	0.371	2.05 ± 0.05
5	0.1 M THAP	0.1 M $LiClO_4$	0.379	1.2 ± 0.1

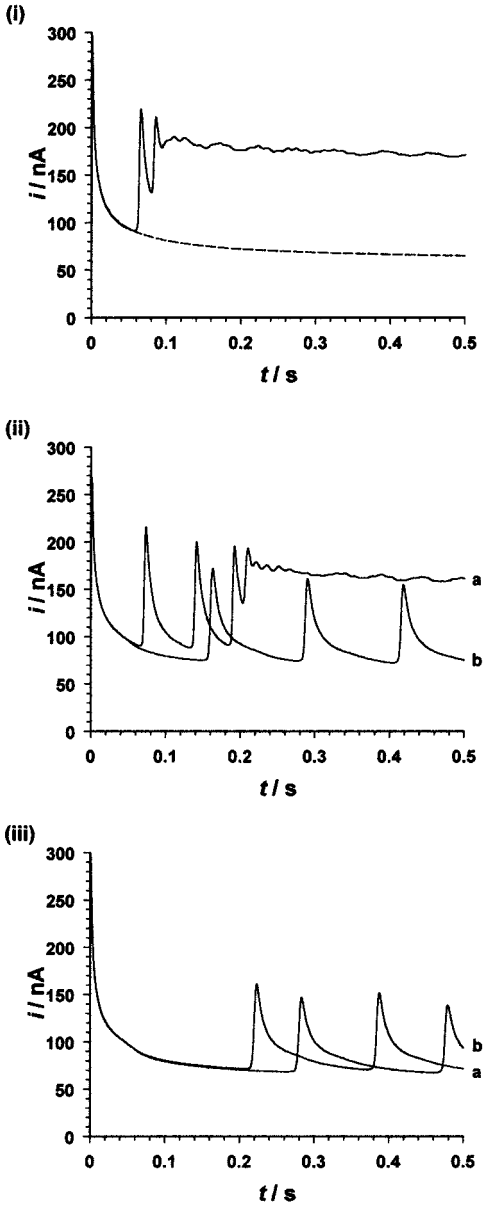

Figure 10. Instabilities in the potential-step current−time response for the diffusion-limited oxidation of Fc at a 25 μm diameter UME positioned close to the DCE/aqueous interface. The DCE phase contained 10 mM Fc and 0.1 M TBAP, whereas the aqueous solution contained 0.1 M $LiClO_4$. The ambient temperature was 24 °C. In (i) the dashed curve is the current−time response for the bulk solution, while the solid curve is the first measurement with the UME positioned ~25 μm from the interface. The remaining data were recorded with the UME moved further from the interface in sequential steps of 2 μm (iia), 5 μm (iib), 2.5 μm (iiia), and 2.5 μm (iiib).

range of solution conditions that have been employed in studies of ET at ITIES, using the $DCMFc/DCMFc^+$ as the redox couple in the organic phase.[11] The organic solution contained 10 mM DCMFc and either 0.1 M TBAP or 0.1 M THAP. The aqueous phase contained 0.1 M $LiClO_4$ or 0.01−0.1 M $NaClO_4$, either with or without 0.1 M NaCl. In general, DPSC data obtained for tip−interface separations of 4.4−14.6 μm were found to be in close agreement with the theoretical predictions for no transfer of $DCMFc^+$ across the interface, over the full range of conditions employed. By using a longer switching time, t_{sw} = 1.138 s, K_e < 0.01 was deduced.

Interfacial Turbulence Induced by Local SECM Measurements. Under certain critical conditions of ambient temperature and concentration of redox mediator, dynamic instabilities of the ITIES were detected, accompanying the local generation of the oxidized ferrocene species near to the interface. These instabilities took the form of deformations and oscillations of the interface, which were observable by video microscopy, and corresponding periodic fluctuations in the current−time response of the UME. The instabilities were clearly associated with the electrochemical generation of the species at the UME and ceased when the potential was stepped back to 0.0 V versus AgQRE or jumped to open circuit.

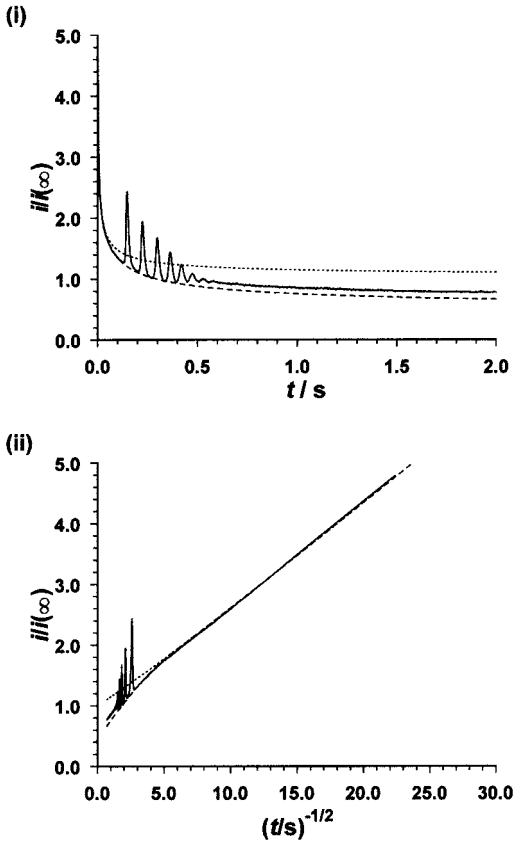

Figure 11. Transient response for a 25 μm diameter UME jumped to a potential for the diffusion-controlled generation of Fc^+, via the oxidation of Fc, while positioned close to a DCE/aqueous interface. The data are shown as plots of $i/i(\infty)$versus (i) t and (ii) $t^{-1/2}$ (solid lines). The DCE solution contained 5 mM Fc and 0.1 M TBAP and the aqueous phase contained 0.1 M $LiClO_4$. The ambient temperature was 23 °C. The dotted curves show the measured response with the UME positioned in the bulk organic phase. The dashed curves show the simulated response for the hindered diffusion of Fc to the tip for d = 16.4 μm.

It is well established that the transfer of a solute across liquid/liquid interfaces may induce motion of the interface, and thereby enhance mass transfer rates.[62−64] This phenomenon has important implications in solvent extraction systems and is a manifestation of the Marangoni effect,[62,65] where local variations of any quantity that affects the interfacial tension—such as interfacial concentration, temperature, or electrical properties—can lead to interfacial convection.[62,66−71] Marangoni flow of fluid has been induced electrochemically[70] and high amplitude periodic oscillations have been observed in SECM approach curve data, for an UME that was moved close to a water/bromobenzene interface where a film formed between $Ru(CN)_6^{4-}$ and TBA^+ or THA^+.[9] The tip current oscillations were attributed to the advancing tip trapping a thin unstable water layer as it moved into the organic phase, the thickness of this water layer changing periodically.

For the three ferrocene species examined in this study, perturbation of the interface was most prevalent for Fc^+ transfer.

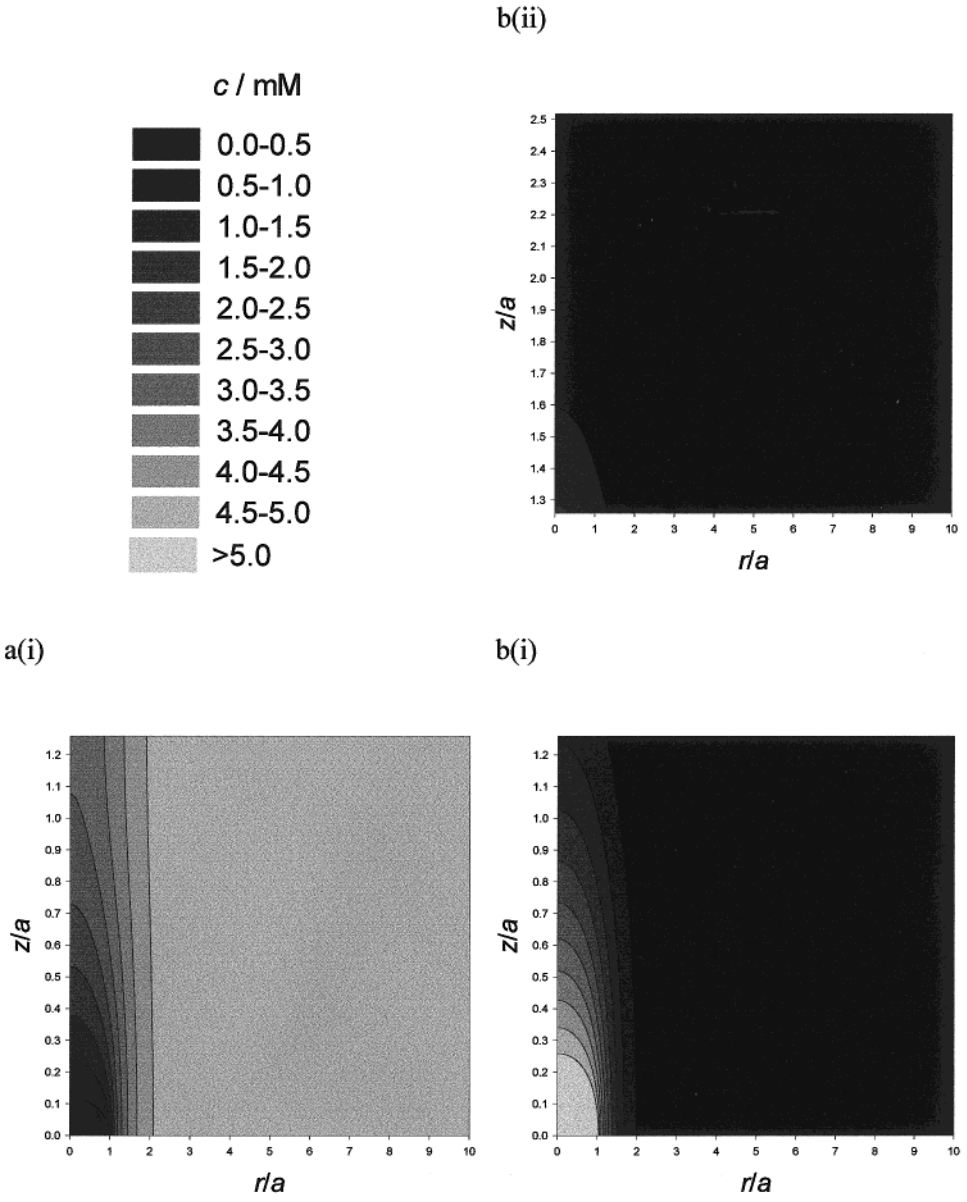

Figure 12. Concentration profiles of Fc (a(i)) and Fc^+ (b(i)) in the DCE phase and the concentration profile of Fc^+ in the aqueous phase (b(ii)), at the time corresponding to the onset of the oscillation in the current response in Figure 11, $t_{osc} = 0.119$ s.

In general the disturbance of the interface was most pronounced for higher concentrations of Fc (typically > 5 mM) and larger UMEs, as the ambient temperature increased (T > 23 °C) and for a freshly contacted liquid/liquid interface. Examples of periodic fluctuations induced by SECM were recorded in several hundred cases. Figure 10 shows transient data for a 10 mM Fc solution observed with the UME stationed at increasing distances from the interface. At the closest tip−interface distance (d = 25 μm) the current suddenly surges, after a period of ca. 50 ms elapses following the initial potential step. The ITIES was observed, by video microscopy, to move to within ~15 μm from the electrode and appeared to remain there for the duration of the potential step. Although this diminishes the tip substrate gap, the corresponding current response of the UME during this time shows an almost constant, enhanced flux, which we attribute to local convection transporting fresh Fc to the interface for oxidation (a consequence of the Marangoni phenomenon). If only the normal diffusion mechanism was operating, one would expect the current to decrease as the tip/substrate distance decreased.[72]

As the tip was moved away from the interface (Figure 10ii and iii) the time corresponding to the initial current surge was found to increase. Moreover, for the further distances, sustained regular periodic current oscillations resulted whose frequency decreased with increasing tip to interface distance. These observations indicate that the instabilities may depend on the interfacial concentration of Fc and Fc^+, which in turn depends on the tip to interface distance and time.

Under less extreme conditions, so that the transient response prior to disturbance sensed the hindered diffusion of Fc to electrode, it was possible to fit the current−time data to provide an accurate value of the tip−interface distance. Using the theoretical model outlined earlier in this paper, it was then possible to simulate concentration profiles of Fc and Fc^+ for the time corresponding to the onset of the first oscillation. An example of transient data for which this was possible is shown in Figure 11, which fits to d = 16.4 μm. The corresponding simulated concentration profiles for Fc and Fc^+ at the time when the oscillation of the ITIES is initiated ($t_{osc} = 0.119$ s) are shown in Figure 12. These plots demonstrate that the diffusion profile

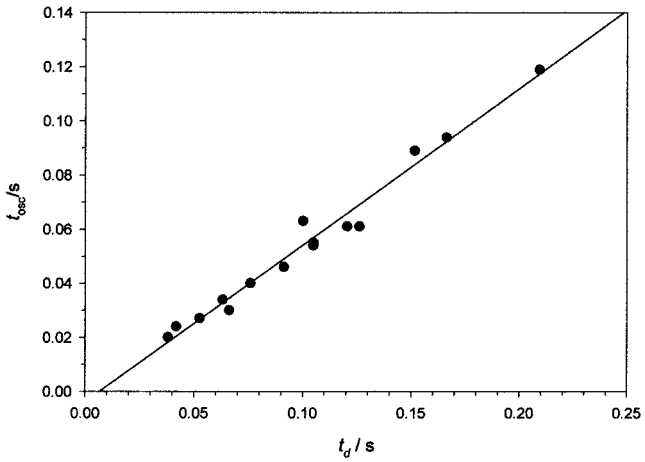

Figure 13. Comparison of the measured time corresponding to the start of the interfacial fluctuation, t_{osc}, and the approximate time for Fc^+ to traverse the tip−interface gap, calculated from $t_d = \{d^2\}/\{2D_{Fc^+,DCE}\}$, using $D_{Fc^+,DCE} = 6.4 \times 10^{-6}$ cm^2 s^{-1}, for a range of tip−interface separations examined. These experiments were performed using a 25 μm diameter UME. The DCE solution contained 5 mM Fc and 0.1 M TBAP while the aqueous phase comprised 0.1 M $LiClO_4$. Measurements were made at $T = 23$ °C. The solid line shows the best fit to the data.

of Fc^+ has just intercepted the ITIES at this time. For a series of measurements made under the same general conditions, but using a range of tip−interface separations there was strong linear correlation between t_{osc} and the time required for the diffusion profile of Fc^+ to reach the interface ($t_d = \{d^2\}/\{2D_{Fc^+}\}$), as shown in Figure 13. This again points to the fact that the interaction of tip-generated Fc^+ with the interface is responsible for the observed current oscillations.

As outlined earlier, there are many factors associated with Fc^+ (and ClO_4^-) transfer that could alter the surface tension of the liquid/liquid interface and so induce interfacial convection. For example, local changes in temperature may occur due to ion hydration especially given the rather higher dissolution flux. Additionally, there is the possibility of variations in interfacial potential[61] and $FcClO_4$ precipitation at the interface. To investigate the latter, the solubility of a ferrocenium salt in aqueous solutions containing 0.1 M $LiClO_4$, was examined by UV/visible spectrophotometry. The extinction coefficient $\epsilon(251\text{ nm}) = 11968$ M^{-1} cm^{-1} was determined from measurements of the absorbance of several dilutions of a stock solution containing 0.5 mM $FcPF_6$ and 0.1 M $LiClO_4$. This value for ϵ is consistent with literature data.[73,74] The concentration of Fc^+ in an aqueous solution that was saturated with $FcPF_6$ was determined as 12.1 mM at 21.5 °C and 10.5 mM at 27 °C from measured absorbances of 0.602 and 0.523 respectively of a 240-fold dilution of the saturated solution. This decrease in solubility with increasing temperature is consistent with the observation of increasing probability for oscillations with increasing temperature. These values are close to the previously reported solubility of 9.9 mM for $FcPF_6$ in water at $T = 298.2$ K. However, these results should be treated with some caution since direct solubility measurements of ferrocenium salts may involve colloidal solutions or fine suspensions,[75] which would lead to an overestimate of the concentration of Fc^+ by UV−vis spectroscopy. Since the ITIES is a transition region in which the chemical composition (e.g., ClO_4^- distribution) and related physical properties change abruptly, the solubility of Fc^+ at the ITIES may also vary from the bulk solution values. The local precipitation of $FcClO_4$ at the ITIES changing the local interfacial tension is therefore a possible explanation of the oscillations observed.

Conclusions

SECM−DPSC has been shown to be a powerful approach for studying reversible phase transfer reactions across ITIES. The technique complements SECMIT which may also be used to study reversible phase transfer.[34] DPSC has advantages in that species that might otherwise be unstable in the bulk solution can be electrogenerated for short measurement periods. Moreover, the time scale of the DPSC measurement may be readily controlled by varying the switching time. In principle, for interfacial transfer processes characterized by moderate to fast kinetics it should be possible to determine the partition coefficient and rate constant independently by using, respectively, long and short switching times.

The use of SECM−DPSC experimentally has been demonstrated through studies of the partitioning of oxidized ferrocene derivatives across DCE/water interfaces, which have been found to be rapid diffusion-limited processes in the case of ferrocene and dimethylferrocene under the experimental conditions, with ClO_4^- in excess in each phase. The interfacial instabilities that are observed in these experiments under conditions of higher temperature and concentration of the ferrocene mediator have been investigated by SECM. These preliminary results show that SECM is a useful tool for locally initiating and monitoring fluctuations of the interface and suggest that further studies would be profitable. A cautionary note also has to be made of the possible complications that may arise in studies of liquid/liquid interfaces by SECM, due to the local nature of the technique. This paper has demonstrated that rapid transient techniques allow such local convective effects to be identified.

Acknowledgment. We are grateful to the EPSRC for support of this work.

References and Notes

(1) Volkov, A. G., Deamer, D. W., Eds. *Liquid/Liquid Interfaces: Theory and Method*; CRC Press: Boca Raton, 1996.

(2) Girault, H. H.; Schiffrin, D. J. *Electrochemistry of Liquid−Liquid interface* in *Electroanalytical Chemistry*; Bard, A. J., Ed.; Marcel Dekker: New York, 1989; Vol. 15, p 1.

(3) Samec, Z.; Marecek, V.; Weber J. *J. Electroanal. Chem.* **1979**, *100*, 841.

(4) Cunnane, V. J.; Geblewicz, G.; Schiffrin, D. J. *Electrochim. Acta* **1995**, *40*, 3005.

(5) Hanzlík, J.; Hovorka, J.; Samec, Z. Toma, S. *Collect. Czech. Chem. Commun.* **1988**, *53*, 903.

(6) Chen, Q.-Z.; Iwamoto, K.; Seno, M. *Electrochim. Acta* **1991**, *36*, 291.

(7) Cheng, Y. F.; Schiffrin, D. J. *J. Chem. Soc., Faraday Trans.* **1993**, *89*, 199.

(8) For recent reviews, see: (a) Amemiya, S.; Ding, Z. F.; Zhou, J. F.; Bard, A. J. *J. Electroanal. Chem.* **2000**, *483*, 7. (b) Barker, A. L.; Slevin, C. J.; Unwin, P. R.; Zhang, J. *Scanning Electrochemical Microscopy as a Local Probe of Chemical Processes at Liquid Interfaces* in *Liquid Interfaces in Chemical, Biological and Pharmaceutical Applications*; Volkov, A. G., Ed.; Marcel Dekker: New York, 2001; Vol. 95, p 283.

(9) Tsionsky, M.; Bard, A. J. Mirkin, M. V. *J. Phys. Chem.* **1996**, *100*, 17881.

(10) Barker, A. L.; Unwin, P. R.; Amemiya, S. Zhou, J. F.; Bard, A. J. *J. Phys. Chem. B* **1999**, *103*, 7260.

(11) Zhang, J.; Barker, A. L. Unwin, P. R. *J. Electroanal. Chem.* **2000**, *483*, 95.

(12) Samec, Z.; Marecek, V.; Weber, J. *J. Electroanal. Chem.* **1977**, *96*, 245.

(13) Samec, Z.; Marecek, V.; Weber, J. *J. Electroanal. Chem.* **1979**, *103*, 11.

(14) (a) Shi, C.; Anson, F. C. *Anal. Chem.* **1998**, *70*, 3114. (b) Shi, C.; Anson, F. C *J. Phys. Chem. B* **1998**, *102*, 9850. (c) Shi, C.; Anson, F. C. *J. Phys. Chem. B* **1999**, *103*, 6283.

(15) Ding, Z.; Fermin, D. J.; Brevet, P.-F.; Girault, H. H. *J. Electroanal. Chem.* **1998**, *458*, 139.

(16) Samec, Z.; Marecek, V.; Weber, J.; Homolka, D. *J. Electroanal. Chem* **1981**, *126*, 105.
(17) Quinn, B.; Lahtinen, R.; Murtomäki, L.; Kontturi, K. *Electrochim. Acta* **1998**, *44*, 47.
(18) Makrlik, E. *Z. Phys. Chem.* (*Leipzig*) **1987**, *168*, S. 212.
(19) Kontturi, A. K.; Kontturi, K.; Murtomäki, L.; Schiffrin, D. J. *J. Chem. Soc., Faraday Trans.* **1990**, *86*, 931.
(20) Geblewicz, G.; Kontturi, A. K.; Kontturi, Schiffrin, D. J. *J. Electroanal. Chem.* **1987**, *217*, 261.
(21) Ding, Z.; Wellington, G.; Brevet, P.-F.; Girault, H. H *J. Phys. Chem.* **1996**, *100*, 10658.
(22) Kakiuchi, T.; Takasu, Y. *J. Phys. Chem. B* **1997**, *101*, 5963.
(23) Kakiuchi, T.; Ono, K.; Takasu, Y. *Anal. Chem.* **1998**, *70*, 4152.
(24) Ding, Z.; Wellington, G.; Brevet, P.-F.; Girault, H. H. *J. Electroanal. Chem.* **1997**, *420*, 35.
(25) (a) Nakatani, K.; Uhida, T.; Misawa, H.; Kitamura, N.; Masuhara, H. *J. Phys. Chem.* **1993**, *97*, 5197. (b) Nakatani, K.; Uchida, T.; Misawa, H.; Kitamura, N.; Masuhara, H. *J. Electroanal. Chem.* **1994**, *367*, 109. (c) Nakatani, K.; Wakabayashi, M.; Chikama, K.; Kitamura, N. *J. Phys. Chem.* **1996**, *100*, 6749. (d) Terui, N.; Nakatani, K.; Kitamura, N. *J. Electroanal. Chem.* **2000**, *494*, 41.
(26) Marcus, R. A. *J. Chem. Phys.* **2000**, *113*, 1618.
(27) Slevin, C. J.; Macpherson, J. V.; Unwin, P. R. *J. Phys. Chem. B* **1997**, *101*, 10851.
(28) Bard, A. J.; Unwin, P. R.; Wipf, D. O.; Zhou, F. *Am. Inst. Phys., Conf. Proc.* **1992**, *241*, 235.
(29) Bard, A. J.; Denuault, G.; Dornblaser, B. C.; Friesner, R. A.; Tuckerman, L. S. *Anal. Chem.* **1991**, *63*, 1282.
(30) Saito, Y *Rev. Polarogr. Jpn.* **1968**, *15*, 177.
(31) Peaceman, D. W.; Rachford, H. H. *J. Soc. Ind. Appl. Math.* **1955**, *3*, 28.
(32) (a) Heinze, J. *J. Electroanal. Chem.* **1981**, *124*, 73. (b) Heinze, J. *Ber. Bunsen-Ges. Phys. Chem.* **1981**, *85*, 1096. (c) Heinze, J. *Ber. Bunsen-Ges. Phys. Chem.* **1986**, *90*, 1043.
(33) (a) Unwin, P. R.; Bard, A. J. *J. Phys. Chem.* **1991**, *95*, 7814. (b) Bard, A. J.; Mirkin, M. V.; Unwin, P. R.; Wipf, D. O. *J. Phys. Chem.* **1992**, *96*, 1861. (c) Unwin, P. R.; Bard, A. J. *J. Phys. Chem.* **1992**, *96*, 5035.
(34) Barker, A. L.; Macpherson, J. V.; Slevin, C. J.; Unwin, P. R. *J. Phys. Chem. B* **1998**, *102*, 1586.
(35) Martin, R. D.; Unwin, P. R. *J. Electroanal. Chem.* **1997**, *439*, 123.
(36) Barker, A. L. Ph.D. Thesis, University of Warwick, Coventry, U.K., 2000.
(37) Shao, Y.; Mirkin, M. V.; Rusling, J. F. *J. Phys. Chem. B* **1997**, *101*, 3202.
(38) Bard, A. J.; Lund, H., Ed. *Encyclopedea of Electrochemistry of the Elements*; Marcel Dekker: New York, 1979; Vol. 111, p 25
(39) Bond, A. M.; McLennan, E. A.; Stojanovic, R. S.; Thomas, F. G. *Anal. Chem.* **1987**, *59*, 2853.
(40) Bond, A. M.; Henderson, T. L. E.; Mann, D. R.; Mann, T. F.; Thormann, W.; Zoski, C. G. *Anal. Chem.* **1988**, *60*, 1878.
(41) Noviandri, I.; Brown, K. N.; Fleming, D. S.; Gulyas, P. T.; Lay, P. A.; Masters, A. F.; Phillips, L. *J. Phys. Chem. B* **1999**, *103*, 6713.
(42) Bond, A. M.; Oldham, K. B.; Zoski, C. G. *J. Electroanal. Chem.* **1988**, *245*, 71.
(43) Mirkin, M. V.; Bard, A. J. *Anal. Chem.* **1992**, *64*, 2293.
(44) Elschenbroich, Ch.; Salzer, A. *Organometallics: A Course Introduction*; VCH Verlagsgesellschaft: Weinheim, 1989.
(45) Kuwana, T.; Bublitz, D. E.; Hoh, G. *J. Am. Chem. Soc.* **1960**, *82*, 5811.
(46) Kolthoff, I. M.; Thomas, F. G. *J. Phys. Chem.* **1965**, *69*, 3049.
(47) Geng, L.; Ewing, A. G.; Jernigan, J. C.; Murray, R. W. *Anal. Chem.* **1986**, *58*, 852.
(48) Sato, M.; Yamada, T.; Nishimura, A. *Chem. Lett.* **1980**, 925.
(49) Bashkin, J. K.; Kinlen, P. J. *Inorg. Chem.* **1990**, *29*, 4507.
(50) Zara, A. J.; Machado, S. S.; Bulhões, L. O. S.; Benedetti, A. V.; Rabockai, T. *J. Electroanal. Chem.* **1987**, *221*, 165.
(51) Prins, R.; Korswagen, A. R.; Kortbeek, A. G. T. G. *J. Organomet. Chem.* **1972**, *39*, 335.
(52) Hanzlík, J.; Samec, Z.; Hovorka, J. *J. Electroanal. Chem.* **1987**, *216*, 303.
(53) Hubbard, A. T.; Anson, F. C. *Electroanalytical Chemistry*; Bard, A. J., Ed.; Marcel Dekker: New York, 1970; Vol. 4.
(54) McDuffie, B.; Anderson, L. B.; Reilley, C. N. *Anal. Chem.* **1966**, *38*, 883.
(55) McDuffie, B.; Anderson, L. B.; Reilley, C. N. *Anal. Chem.* **1966**, *38*, 1881.
(56) Macpherson, J. V.; Unwin, P. R. *Anal. Chem.* **1997**, *69*, 2063.
(57) Daschbach, J. Blackwood, D., Pons, J. W, Pons, S *J. Electroanal. Chem.* **1987**, *237*, 269.
(58) Kamau, G. N., Saccucci, T. M., Gounill, G., Nassar, A.-E. F., Rusling, J. F. *Anal. Chem.* **1994**, *66*, 994.
(59) Barker, A. L.; Unwin, P. R. In preparation.
(60) Ohsawa, Y.; Aoyagui, S. *J. Electroanal. Chem.* **1982**, *136*, 353.
(61) Selzer, Y.; Mandler, D *J. Phys. Chem. B* **2000**, *104*, 4903.
(62) Sawistowski, H. In *Recent Advances in Liquid−Liquid Extraction*; Hanson, C., Ed.; Pergamon: Oxford, 1971; p 293.
(63) Lewis, J. B.; Pratt, H. R. C. *Nature* **1953**, *171*, 1156.
(64) Maroudas, N. G.; Sawistowski, H. *Nature* **1960**, *188*, 1186.
(65) Scriven, L. E.; Sternling, C. V. *Nature* **1960**, *187*, 186.
(66) Chaudhury, M. K.; Whitesides, G. M. *Science* **1992**, *256*, 1539.
(67) Austin, L. J.; Banczyk, L.; Sawistowski, H. *Chem. Eng. Sci.* **1971**, *26*, 2120.
(68) Nakache, E.; Dupeyrat, M. *Faraday Discuss. Chem. Soc.* **1984**, *77*, 189.
(69) Magome, N. Yoshikawa, K. *J. Phys. Chem.* **1996**, *100*, 19103.
(70) Bennett, D. E.; Gallardo, B. S.; Abbott, N. L. *J. Am. Chem. Soc.* **1996**, *118*, 6499.
(71) Lee, H. J.; Fermín, D. J.; Corn, R. M.; Girault, H. H. *Electrochem. Commun.* **1999**, *1*, 190.
(72) Kwak, J.; Bard, A. J. *Anal. Chem.* **1989**, *61*, 1221.
(73) Wilkinson, G.; Rosenblum, M.; Whiting, M. C.; Woodward, R. B. *J. Am. Chem. Soc.* **1952**, *74*, 2125.
(74) Rosenblum, M. *Chemistry of the Iron Group Metallocenes*, *Part 1*; John Wiley & Sons: New York, 1965; Chapter 2.
(75) Blundell, N. J.; Burgess, J. *Inorg. Chim. Acta* **1990**, *173*, 5.